ANNUAL CYCLES OF SST-TPW OVER TROPICAL OCEANS: INSIGHTS FROM TRMM ANALYSIS

Gian Luigi Liberti[(1)], Prashant Goswami[(2)]

[(1)] ISAC-CNR, Via Fosso del Cavaliere 100, I-00133, Rome, ITALY, Email:g.liberti@isac.cnr.it
[(2)] CSIR-4PI, Wind Tunnel Road, Bangalore 560037, India, Email: : Goswami@cmmacs.ernet.in

ABSTRACT

This study focuses on the relative phase between the average annual cycles of Sea Surface Temperature (SST) and Total Precipitable Water (TPW) over tropical/subtropical Oceans (40°S-40°N). Average annual cycles, for 0.25°x0.25° grid boxes in the study area, are obtained from the reasonably long database (Dec.1997-Oct.2014) from a single MW and relatively stable instrument (TMI) able to estimate both variables in absence of precipitation.

From a first qualitative analysis of the SST-TPW relationships emerged a variety of behaviours depending on a combination of large scale general atmospheric circulation patterns and smaller scale influence of land surfaces. A quantitative description of such complexity is attempted by introducing a set of variables computed on the basis of the curve described by the average annual cycles in the SST-TPW plane. A semi-objective procedure to define sub-regions of the Tropical oceans on the basis of the relationship of SST and TPW annual cycles is finally explored.

1. INTRODUCTION

Total Precipitable Water vapour (TPW) and Sea Surface Temperature (SST) are key atmospheric variables for many applications in different fields covering different spatio-temporal scales. Analysis of observed variability of the TPW and its association with the SST at different scales can provide valuable insights into processes like the air-sea interaction or the regional hydrological cycle. Over the Oceans, in particular the Tropical ones, TPW and SST are expected to be strongly coupled. Reference [1] obtained analytically a functional form relating the TPW to the SST based on an approximation of Clausius-Clapeyron equation for the saturation water vapour (WV) pressure making a set of assumptions on the surface relative humidity and on the WV and atmosphere scale heights. Successive studies [e.g. 2-4] refined the approach with the help of observations pointing out the spatial variability of the parameters used in the equation that reflect for example the variability of WV vertical distribution over the oceans.

A first attempt to explore the information content, in the difference between the observed TPW and expected TPW average value as estimated from SST, to infer WV vertical distribution properties is reported in [5]. A detailed description of the spatio-temporal variability of the SST-TPW relationship can improve the accuracy of estimation of atmosphere-ocean latent heat fluxes derived from satellite passive radiometry. While the spatial variability of SST-TPW relationship has been already explored [e.g. 3-4] its temporal variability is still poorly documented [6] and could explain the residual variability observed in locally derived relationships. This study focuses on the analysis of the spatially detailed (0.25°x0.25°) average annual cycles of SST and TPW over tropical/subtropical Oceans (40°S-40°N). The dynamical coupling between TPW and SST is expected to reflect in their annual cycles and in the relative amplitude/phase relationship.

The spatially detailed description of average SST and TPW annual cycles is obtained from the long-term (Dec.1997 to Oct.2014) dataset of geophysical products distributed by the Remote Sensing Systems (RSS) (www.remss.com) retrieved from microwave passive radiometric observations from the Tropical Rainfall Measuring Mission (TRMM) Microwave Imager (TMI) [7]. The dataset is described in Section 2. The analyses performed and the results are reported in Section 3. Conclusions and perspective for further developments of the study are reported in Section 4.

2. DATA SET DESCRIPTION

The TMI-derived TPW and SST estimates used in this study to describe the average annual cycles are from the TMI Version 4 (released September 13th, 2006) products, available from Remote Sensing Systems (RSS) (www.remss.com). Data from December 1997 to October 2014 have been used.

TPW and SST values are archived in daily files containing also other retrieved geophysical products: 10 m wind intensity from 2 different algorithms, cloud liquid water and precipitation. All products cover the 40°S-40°N latitude belt and are given on a 0.25°x0.25° regular grid obtained by remapping the antenna temperature with an optimal interpolation scheme. A daily file contains, for each grid point and variable, no more than two observations per day: one for the descending and one for the ascending orbit. For a given type of orbit, more than two observations per day are possible because of the overlap between the first and the last orbit segments of the day or because the overlap of contiguous orbits, close to the upper and lower latitude TMI observing limits. In both cases the newer values of the retrieved parameters are reported loosing part of the

diurnal sampling information contained in the original TMI observations.

Each variable is stored as a single byte using the values 0-250 and leaving the last 5 values (251 to 255) for quality flags. For the TPW, having set the range from 0 to 75 mm, the resulting numerical resolution is 0.3 mm. For the SST the range is -3÷34.5°C with a numerical resolution of 0.15°C.

The algorithm used to retrieve all geophysical parameters is described in [8-9]. It was originally developed for SSMI [10] and optimized for the TMI and AMSRE instruments, both having lower frequencies channels (<19 Ghz) with sensitivity to the SST. The available documentation mostly refers to the adaptation of the original algorithm to the AMSRE with little mention to the specific issues concerning the TMI. In the following, a short description of the inversion algorithm, in the parts relevant for our study, is reported.

The algorithm is based on a two stage regression between Tb's and geophysical parameters using as ancillary information, the wind direction from NCEP (National Centers for Environmental Prediction) GDAS (Global Data Assimilation System) analysis and salinity values from the National Oceanographic Data Center (NODC) World Ocean Atlas [11]. For TPW and cloud liquid water the channels used are the 19, 22 and 37 Ghz.

All regression coefficients are obtained from a training set of Tb's originated from a set of geophysical scenes simulated with a Radiative Transfer Model (RTM). The geophysical scenes are generated starting from a set of 42195 radiosondes from weather ships or from 56 sites on small islands (37650 launched between 1987 and 1990 the remaining at the latest in 2000). For each profile: cloud water from 0 to 0.3 mm is added, the SST varied +/-5.5°C from the Reynolds climatology [12] the wind speed varied from 0-40 m/s and the wind direction 0-360° in 20° steps.

The accuracy of the SST and TPW RSS TMI-derived products is documented in few validation studies [13-16].

3. RESULTS

For each ocean 0.25°x0.25° grid box in the TMI geographical domain [40°S-40°N] the average annual cycle of all retrieved geophysical variables was computed together with other relevant statistics for geophysical variable and also (see below) for the Local Solar Time (LST) at which the observations were taken. For leap years data from the February 29 were associate to March 1. Only observations with valid SST estimations (No precipitation and no land contamination) were used in the computation of the annual cycles of both variables. In principle, the data base contains valid TPW values also when the SST estimation is absent. This is due to the fact that TPW estimation is based on higher frequency, and as a consequence smaller FOV, channels compared to the SST for what concern the land contamination. In addition, in presence of light precipitation an estimation of TPW is still given, however [16] showed that accuracy of TPW, as estimated from the comparison against radiosonde derived one, decrease drastically in presence of precipitation. *Fig.1* shows the map of valid observations (as % of the maximum value in the domain) used for the definition of the average annual cycles. As expected, the geographical distribution shows the typical patterns of occurrence of precipitation.

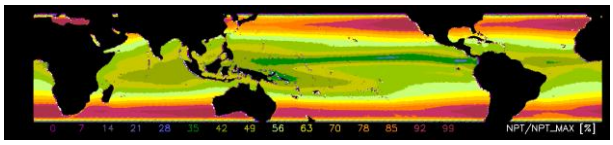

Figure.1. Number of valid observations used for the definition of annual cycles.

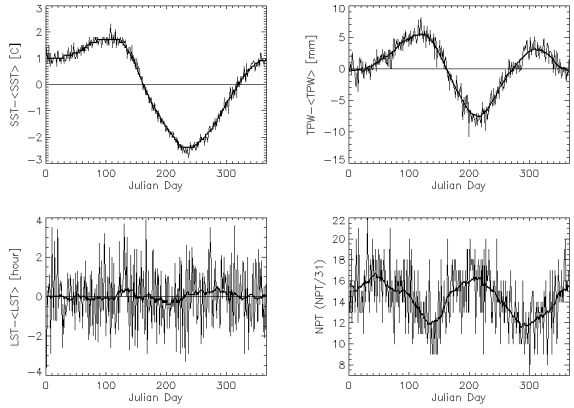

Figure.2. Example (box 3.5°N- 0.25°E) of average annual cycles (reported as anomaly of the overall average value) for SST, TPW, LST and NPT. Thin lines correspond to the average computed over the single Julian day while thick is the corresponding value computed over a +/-15 days window.

The non-synchronous orbit of the TRMM mission allows to sample of the diurnal cycle of the retrieved geophysical variables. Fig. 2 shows an example of average annual cycles of SST, TPW, LST and Number of valid observations (NPT). The thin line correspond to the average value using strictly observations for a given Julian day in the computation of the average. The average LST has an high frequency variability that also depends from the latitude. Because in this study there is no interest on diurnal variability and also because it has been shown that, despite correction applied, there may be a residual effect of diurnal warming of the instrument [17-20] in the retrieved geophysical variable, for each Julian day the average values are computed over a +/-15 days window (thick lines in Fig.2). Given the characteristics of the dataset this means that the max of observations used to compute a single Julian day average value is 1054.

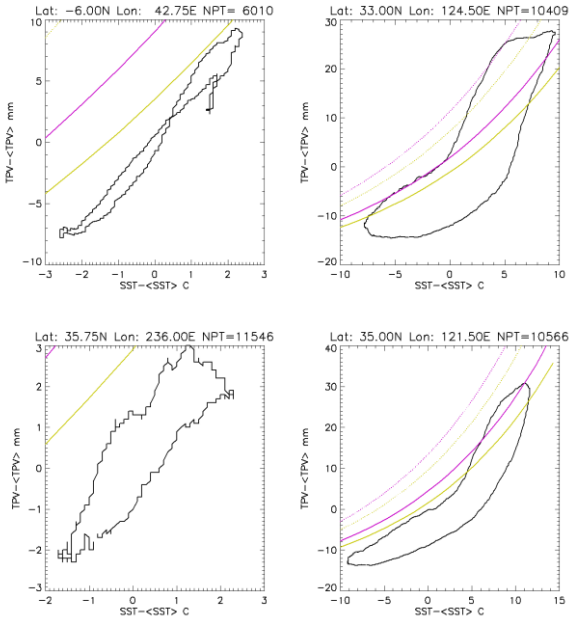

Figure.3. Examples of annual cycles for boxes with relatively large valid of valid observations (NPT>6000) that have minimum (left) or maximum (right) of one of the defined parameters: (from top to bottom) Area, Dist. The coloured curvse correspond to the values of the relationship defined in eq. 5 in [1] with: r=0.8(green),0.8(purple), atmospheric scale height=7 km, WV scale height=2 (full line), 3 (dashed line) km.

3.1. Definition of geometrical parameters of the curves and mapping the parameters.

A qualitative visual analysis of the relationship between annual cycles of SST and TPW showed a large variety of behaviours. In order to describe somehow the different curves described in the 2D plan an attempt was done to define a minimum set of scalars that could represent important properties of the curves. Moreover once described such set of variables it is possible to represent their geographical distribution.

A preliminary set of variables has been defined as follow (see Figs. 3 and 4):

- **Area:** the area described from the curve gives an indication on the variability of the SST-TPW relationship during the year. In principle, if a single valid relationship between the two variable exists the area should be 0. Physically the area should (means that energy/mass is stored or lost) there are at least two different branches with two different relationships
- **Perimeter:** together with the maximum Euclidean distance is an estimate of the amplitude of the cycles. In fact, the largest values of this parameter (see Fig. 4)
- **Area/Perimeter:** this parameter is introduced to estimate the *roundness* of the curve. At a first analysis seems to be highly correlated to the area (see Fig. 4).
- **Maximum Euclidean Distance** (*DIST*) between any two points in the curve (should measure the dynamic)

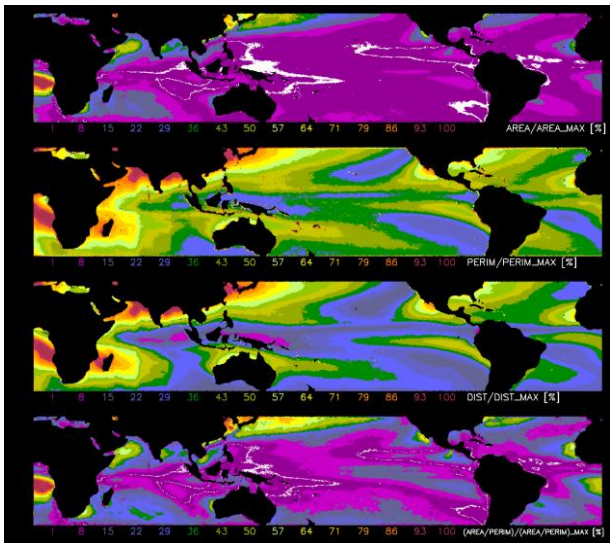

Figure 4.Geographycal distribution of the parameters defined to describe the SST-TPW annual cycles relationship. All colour scales are relative to the maximum value obtained for each mapped parameter.

3.2. Definition of the Subregions

Beside the mapping of properties of the mutual annual cycles an attempt to define sub-regions on the basis of the relationship between the annual cycles of the two variables have been performed. The semi-objective procedure is the following:

0) a candidate reference grid box (in the following named as sub-region centre) is selected as the one with the largest number of valid measurements (11916) with the assumption that a large number of valid measurements gives a good description of the statistics. Practically the grid box with this large number of valid measurements is in the subsidence region off of the west coast of Chile and it represents, from the point of view of TPW a very peculiar regime.
1) once defined the sub-region centre the average Euclidean distance (D) between the curve described, in the SST-TPW plane, by the annual cycles in the sub-region centre and the one in all other grid boxes is computed.
2) a new candidate sub-region centre is defined as the grid box with the maximum residual distance with the additional condition on the number of valid measurements expressed as percentage of the overall maximum (see below).
3) for each grid box the average distance D is computed using as reference the annual cycles from the new centre. If this value is less the previous one the grid box is associated with the current centre and the distance is stored as maximum residual distance.
4) steps 2 and 3 are repeated until the criteria to stop the procedure is reached. In this phase we allowed the definition of up to 50 sub-regions in order to

investigate the behaviour of the procedure and to define, on the basis of this analysis, more objective criteria to stop the definition of new sub-regions.

The condition on the minimum number of valid measurements to be a candidate sub-region centre has been introduced because coastal pixels generally have very peculiar behaviour partly due to the vicinity of the coast but mostly due to the relatively low number of valid measurements used to compute the average annual cycles that results in a noisy description of the annual variability. These factors contribute both in generating large values of *D* and as a consequence locating the sub-regions centres mostly in coastal regions. By introducing a minimum number of valid measurements the possibility to have a candidate sub region centre poorly representative of the oceans is partly reduced. Four values of percentage (0, 25, 50, 75 %) have been tested for the procedure. Fig. 5 shows the residual maximum distance between annual cycles of all grid-boxes and the ones of the sub-regions centres as a function of the number of sub regions and of the minimum number of valid measurements (expressed as % of the overall maximum) for a grid box to be allowed as a candidate sub-region centre. Allowing all grid points as possible candidates (black curve) results in a relatively slow decrease of the maximum residual distance compared with the criteria selecting only highly populated grid points as possible centres (75% red points). However requiring for large numbers of valid measurements does not allow to have as candidate centres grid boxes in regions characterized by large occurrence of precipitation (as for the ITCZ see Fig.1).
Fig.6 shows the position of the first 50 centres resulting for the procedure for the different criteria on the minimum number of valid measurements (same color code as Fig. 5). Even when only grid boxes with large values of valid measurements (75% red) are allowed as centres there is a large occurrence of centres located close to the coasts.

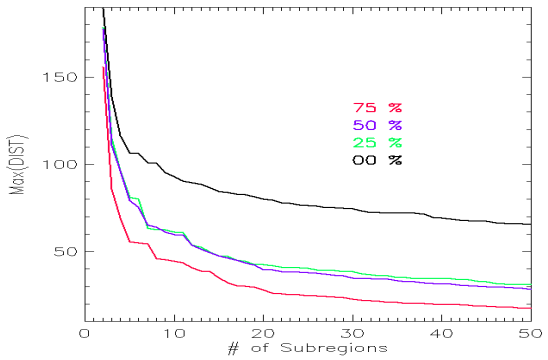

Figure 5. Residual maximum distance between annual cycles of all grid-boxes and the ones of the sub-regions centres as a function of the number of sub regions and of the minimum number of valid measurements (expressed as % of the overall maximum) for a grid box to be allowed as a candidate sub-region centre.

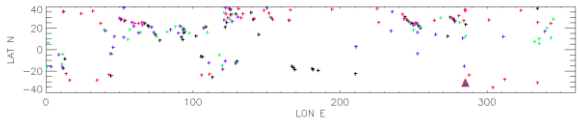

Figure 6 Position of the first 50 candidates sub-region centres. Different colours refer to the minimum valid measurement criteria as in fig.5. The position of the starting subregion centre is represented by a triangle.

Once associated each grid box to a subregion the characteristics of the annual cycle average over the subregion are investigated.
Fig. 7 shows the geographical distribution of the subregions and of the corresponding residual maximum distance for the case of max of allowed subregions = 10 and minimum valid measurements criteria of 75%. Fig. 8 shows the subregion overall average annual cycles for the subregion showed in fig. 7. The classification identify several expected features but fails for example to identify as a specific subregion the ITCZ because of the limitation on minimum number of valid observations.

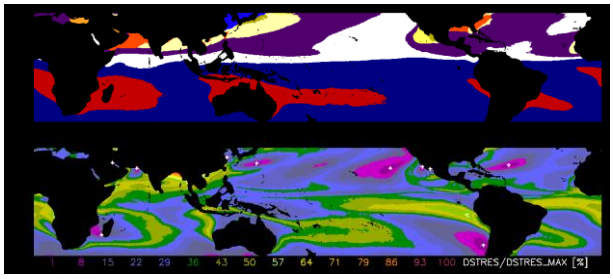

Figure 7. Example of results of sub-regions classification obtained allowing for a max of 10 subregions and a minimum set of valid measurements of 75% of the overall maximum. (Upper panel) Geographical distribution of the subregions.(Lower panel) Map of the residual maximum distanceas a % of the overall maximum (white pluses are the subregion centers).

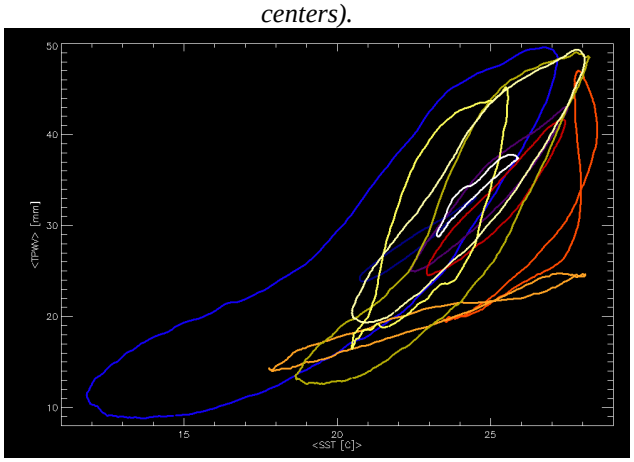

Figure 8. Average annual cycles for the subregions showed in Fig.7.

4. CONCLUSIONS

Despite the large number of important studies on the SST-TPW relationship [e.g.1-6] few aspects of this coupling (e.g. relationship between diurnal cycles [21]) are still poorly explored, mostly for the lack of reliable observations. Reference [3] documented the spatial variability of the SST-TPW relationship over the 40°S-40°N area but in their conclusions they report the need to investigate the temporal dependence of the parameters used to describe the relationship. This study reports a set of preliminary results on the analyses of phasing between average annual cycles of TPW and SST retrieved from the TMI passive radiometer observations over the tropical/sub-tropical (40°S-40°N) oceans.

A large variety of mutual relationships was found by analysing in details the results obtained for each single grid box. An very preliminary attempt to describe in a synthetic form the different behaviours in order to interpret them on the basis of general circulation and climate regimes is reported.

Beside the refinement of the technique presented to analyze and to interpret the observed annual cycles, few questions should be addressed in the successive phases of this study:

- MW passive radiometry allows to estimate the SST also in presence of non precipitating clouds, however in presence of precipitation the TMI product used does not retrieve SST value and even the retrieved TPV has been shown [16] to have a large difference when compared against radiosonde derived values. Therefore we removed all grid boxes with occurring precipitation. As a consequence we expect, beside a different size of the dataset over which the statistics are computed (see Fig. 1) a representation of the regions with high occurrence of precipitation (e.g. the ITCZ) with a bias toward dry regimes. An estimation of possible impact should be somehow attempted.
- The definition of a set of parameters to describe the different relationship should be finalized to obtain a minimum number of relatively independent parameters that should also be easily related to some physical quantity and related processes.
- The semi-objective procedure to define sub-regions should be robustly tested in terms of sensitivity on parameters and criteria to stop.
- The influence of other geophysical variable, particularly the wind speed, contained in the dataset should be documented.
- Finally, investigation of the temporal relationship at a different time scale (diurnal) could be attempted with the same dataset providing an estimation of the residual effect due to instrumental factors [17-20].

AKNOWLEDGMENTS

TMI data are produced by Remote Sensing Systems and sponsored by the NASA Earth Science MEaSUREs DISCOVER Project. Data are available at www.remss.com.

5. REFERENCES

1. Stephens, G.L. (1990). On the relationship between water vapor over the oceans and sea surface temperatures. *J. Climate*, **3**, 634-645.
2. Gaffen, D. J., W. P. Elliott and A. Robock (1992): Relationships between tropospheric water vapor and surface temperature as observed by radiosondes. *Geophys. Res. Lett.*,**19**, 1839–1942.
3. Zhang,C. & Qiu F. (2008). Empirical Relationship between Sea Surface Temperature and Water Vapor: Improvement of the Physical Model with Remote Sensing Derived Data. *J. of Oceanography*, **64**, 163-170.
4. Kanemaru, K. & Masunaga, H. (2013). A Satellite Study of the Relationship between Sea Surface Temperature and Column Water Vapor over Tropical and Subtropical Oceans. *J. Climate*, **26**, 4204–4218
5. Prabhakara, C., Dalu, G., Lo, R.C., & Nath, N.R. (1979). Remote sensing of seasonal distribution of precipitable water vapor over the oceans and the inference of boundary layer structure. *Mon. Wea. Rev.*, **107,**1388-1401.
6. Aumann, H.H., Gregorich, D., Broberg, S., Elliott, D. (2007). Seasonal correlations of SST, water vapor, and convective activity in tropical oceans: a new hyperspectral data set for climate modeling. *Geophys. Res. Lett.*, **34**, L15813
7. Kummerow, C., Barnes, W., Kozu, T., Shiue, J., & Simpson, J., (1998). The Tropical Rainfall MeasuringMission (TRMM) sensor package. *J. Atmos. Ocean. Technol.*, **15**(3), 809–817.
8. Wentz, F.J., & Meissner, T. (2000). AMSR Ocean Algorithm, Version 2, report# 121599A-1, Remote Sensing Systems, Santa Rosa, CA, 66 pp.. online at http://www.remss.com.
9. Wentz, F.J. & Meissner T. (2007) Supplement 1. Algorithm Theoretical Basis Document for AMSR-E Ocean Algorithm. *RSS Tech. Rpt. 051707*, Remote Sensing Systems, Santa Rosa, CA, 6 pp., Available at www.remss.com.
10. Wentz, F.J. (1997). A well calibrated ocean algorithm for special sensor microwave/imager. *J. Geophys. Res.* **102**, 8703-8718.

11. Antonov, J.I., Seidov, D., Boyer, T.P., Locarnini, R.A., Mishonov, A.V., Garcia, H.E., Baranova, O.K., Zweng, M.M. & Johnson, D.R. (2010) *World Ocean Atlas 2009, Volume 2: Salinity.* S. Levitus, Ed. NOAA Atlas NESDIS 69, U.S. Government Printing Office, Washington, D.C. 184 pp.
12. Reynolds, R.W., Smith, T.M., Liu, C., Chelton, D.B., Casey, K.S. & Schlax, M.G. (2007). Daily high-resolution blended analyses for sea surface temperature. *J. Climate*, **20**, 5473-5496.
13. Gentemann, C.L, Wentz, F.J., Mears, C.M. & Smith, D.K. (2004) In-situ validation of TRMM microwave sea surface temperatures. *J. Geophys. Res.*, **109**, C04021.
14. Reynolds, R.W., Gentemann, C.L. & Corlett**,** G.K. (2010). Evaluation of AATSR and TMI satellite SST data", *J. of Climate*, **23**, 152-165.
15. Sajith A., et al. (2007). Evaluation of daily and diurnal signals of total precipitable water (TPW) over the Indian Ocean based on TMI retrieved 3-day composite estimates and radiosonde data." *Int.J.Climatol.* **27**, 761-770.
16. Liberti, G.L., Buzzicotti, M. & C.Transerici, (2012). Validation of TMI derived Total Precipitable Water Vapour with operational soundings. *Proc. Microrad 2012*. Frascati, Italy. 4pp.
17. Geer, A.J., Bauer, P., & Bormann, N. (2010). Solar Biases in Microwave Imager Observations Assimilated at ECMWF. *IEEE Trans. Geosci. Remote Sens.*, **48**(6), 2660-2669.
18. Wentz, F., Ashcroft, P., & Gentemann, C. (2001). Post-launch calibration of the TRMM Microwave Imager, *IEEE Trans. Geosci. Remote Sens.*, **39** (2), 415–422.
19. Biswas, S.W., Gopalan, K., Jones, W.L., & Bilanow, S. (2010). Correction of Time-Varying Radiometric Errors in TRMM Microwave Imager Calibrated Brightness Temperature Products. *IEEE Trans. Geosci. Remote Sens. Letters*, **7**(4), 851-855.
20. Gopalan, K., Jones, L., Biswas, S., Bilanow, S., Wilheit, T. & Kasparis, T. (2009). A time-varying radiometric bias correction for the TRMM Microwave Imager, *IEEE Trans. Geosci. Remote Sens.*, **47**(11), 3722–3730.
21. Clayson, C.A. & Bogdanoff, A.S., (2013). The Effect of Diurnal Sea Surface Temperature Warming on Climatological Air–Sea Fluxes. *J. Climate*, **26**, 2546–2556.